The Behavior of Slab-Column Connections with Modified Shear Reinforcement under Cyclic Load

Riawan Gunadi[1], Bambang Budiono[2], Iswandi Imran[2] & Ananta Sofwan[2]

[1]Civil Engineering Department, Politeknik Negeri Bandung,
Jl. Gegerkalong Hilir, Ds. Ciwaruga, Bandung 40163, Indonesia
[2]Structural Engineering, Faculty of Civil and Environmental Engineering,
Institut Teknologi Bandung, Jl. Ganesa No.10, Bandung 40132, Indonesia
Email: rgunadi@polban.ac.id

Abstract. Generally, slab-column frames show lower stiffness, drift capacity, and ductility as compared to beam-column frames. Under combined gravity and lateral cyclic loading, the lower initial stiffness and stiffness degradation lead to poor structural performance. Therefore, in the current codes, slab-column frames are recommended only for Intermediate Moment Frames with dual systems. The objective of this study is to modify slab-column connection details to enhance seismic performance such that the system can also be used with Special Moment Frames. Four specimens of interior slab-column connection models with the same dimensions and flexural reinforcement were tested under gravity and cyclic lateral loads. One specimen, constructed as control specimen, was designed using standard orthogonal stud rails. The other specimens used newly designed stud rails. The experimental results demonstrated that the modified stud rails significantly improved the specimens' behavior. The experimental results demonstrated that the modified stud rails significantly improve the specimen behavior. The highest ratio of initial stiffness adequacy of specimen with modified stud rail was 131.19% for risk category I/II, while the ratio of the control specimen was 97.94%. The highest relative energy dissipation ratio of specimen with modified stud rail was 33.82%, while the ratio of the control specimen was 25.94%.

Keywords: *gravity load*; *energy dissipation; lateral cyclic load; slab-column connection; stud rail; stiffness.*

1 Introduction

Slab-column frames are favorable because they are economical. However, previous experimental and numerical studies have shown that slab-column frames are not suitable to be used as main lateral force resisting systems in high seismic risk regions [1]. Slab-column frames are very flexible compared to beam-column frames, leading to poor seismic performance. Slab-column connections exhibit lower initial stiffness and more significant stiffness degradation, which also leads to both strength degradation and low energy dissipation under earthquake excitation. Slab-column connections also have a

Received April 30th, 2013, Revised October 23rd, 2013, Accepted for publication December 12th, 2013.
 ISSN: 2337-5779, DOI: 10.5614/j.eng.technol.sci.2014.46.1.2

high potential risk of brittle punching shear failures under gravity-dominated action. All of these structural weaknesses limit the widespread use of slab-column frames. To minimize the risks related to combined gravity and seismic loads, slab-column frames are recommended to be used only for Intermediate Moment Frames [2,3]. Slab-column frames are not recommended to be used in high potential earthquake zones of Seismic Design Category (SDC) D and E, or F for buildings higher than 49 and 30 meters respectively, even though slab-column frames are being used as part of dual systems [2,4].

To improve the behavior of slab-column frames, some experiments have been conducted such as the use of drop panels and shear capital [5], a modified design of the stirrups [5,6], a stirrup cage [7], and stud rail [5,6]. The use of stud rail results in the most favorable solution, but does not solve the problems of low stiffness and energy dissipation. Therefore, a new design of the slab-column frame is required to comply with at least the SDC D for tall buildings.

2 Experimental Research Program

This paper is based on the experimental research reported by Budiono, *et al*. [8] and Gunadi, *et al.* [9]. The research objective was to modify slab shear reinforcement details to enhance the seismic behavior of slab-column frames as part of a dual system (Figure 1) from less to fully ductile. The shear walls were designed to restrain not less than 80% of the total design lateral load. To improve the lateral force capacity of the slab-column frames proportionally from 20 to 25% of the total lateral load, it is necessary to increase the slab thickness or to design the details of the slab plastic hinge, especially the shear reinforcement, to fulfill the acceptance criteria of special moment resisting frames [10]. To solve the problem of detailing the plastic hinge, the shear reinforcement could be fabricated to be precisely detailed. In the future, part of the slab-column connection could be constructed as a precast component.

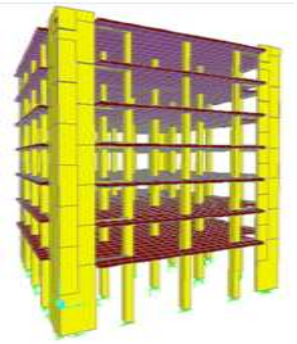

Figure 1 Dual system consisting of shear walls and slab-column frames.

Based on previous researches [5,6], stud rail was used in this research as shear reinforcement of the slab-column connection. The stud rail mainly consisted of stems, strip bases, and anchor heads. Modification of the stud rail was meant to improve the behavior of the slab-column connections in terms of strength, stiffness, and energy dissipation.

The experimental study was conducted at the Structural Mechanics Laboratory of the Engineering Center for Industry of the Institut Teknologi Bandung (ITB), using four specimens of half-scale interior slab-column connection sub-assemblages under combined gravity and cyclic lateral loads [6].

2.1 Material Properties of the Specimen

The steel material properties (Table 1 [8] and Figure 2 [8]) were tested at the Structural Mechanics Laboratory of the Engineering Center for Industry of ITB.

Table 1 The material property of steel bars.

Reinforcement Types	ID	Diameter (mm)	Yield Stress (MPa)
Flexural reinforcements:			
Column reinforcement	(D13)	13.73	390.74
Slab reinforcement	(D8)	7.82	321.50
Stirrups:			
Column stirrup	(D6)	5.90	354.77
Slab stirrup	(D4)	4.45	364.46
Stud rails:			
Shear stud/stem (Figure 2)		7.68	534.3 *)

*) proportional yield stress

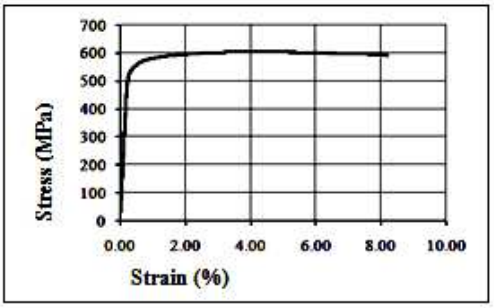

Figure 2 stress-strain relationship of stem material.

The cylindrical compressive strength of the concrete (Table 2 [8]) was obtained at the same day as the slab-column specimens were tested. The tests on

Specimens 1, 2, 3, and 4 were carried out when the concrete was 33, 38, 39, and 37 days old, respectively.

Table 2 Material properties of concrete.

Specimen	Weight (KN/m^3)	Strain at Peak Stress (%)	f'_c (MPa)	
			Range	Average
1	22.46	0.41	41.98 – 50.10	46.21
2	22.62	0.35	42.99 – 50.10	46.16
3	22.70	0.40	39.86 – 50.47	46.18
4	22.64	0.38	28.71 – 36.74	32.72

2.2 Design of the Specimens

The specimens were taken and modified from a prototype interior slab-column connection of a frame with half-scale dimensions [6] as seen in Figures 3 to 5 [9]. All specimens had the same slab thickness of 120 mm.

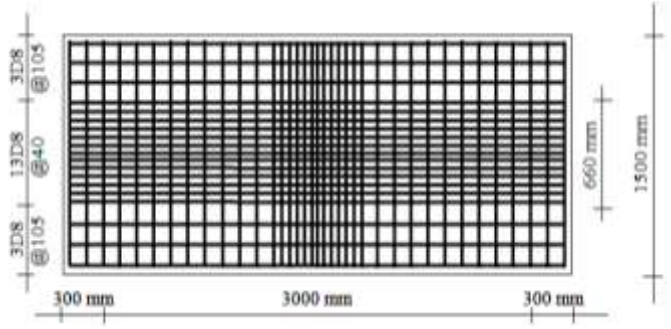

Figure 3 Plan of slab top reinforcement.

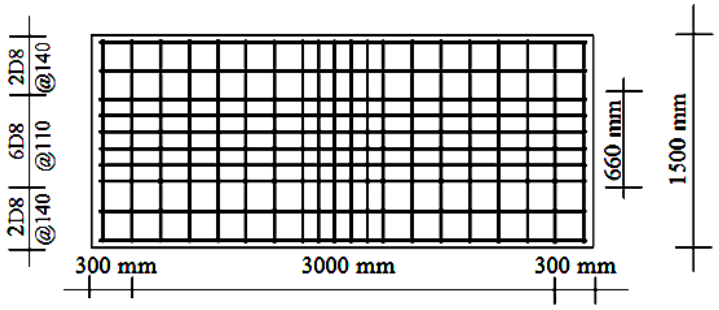

Figure 4 Plan of slab bottom reinforcement.

In the longitudinal direction, 19 and 10 reinforcing steel bars were placed on the top and bottom of the slab, as shown in Figures 3 and 4 [9] respectively.

The longitudinal reinforcement of the column comprised of 12 steel bars with 50 mm spacing of stirrups, as shown in Figure 5.

The stud rails (Figures 6 and 7 [11]) were fabricated at the Mechanical Workshop of Bandung State Polytechnic. The stud rail was designed to ensure that the stem fails prior to the welds connecting the stem to the anchor head and the stem to the strip base. Specimen 1, the control specimen, was designed to use standard orthogonal stud rail [12,13], as shown in Figure 8 [8].

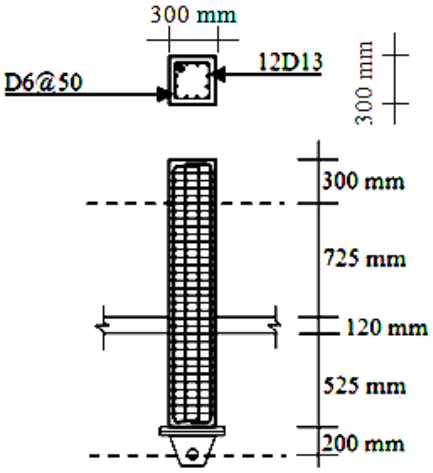

Figure 5 Column reinforcement.

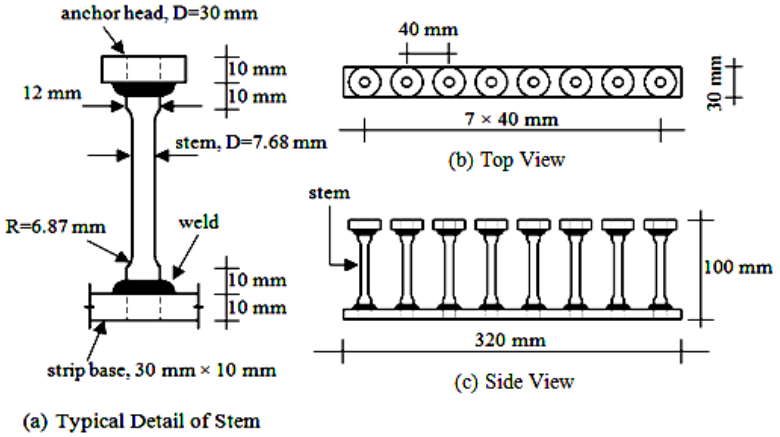

Figure 6 Bottom-up stud rail for specimens 1, 2, and 4 [11].

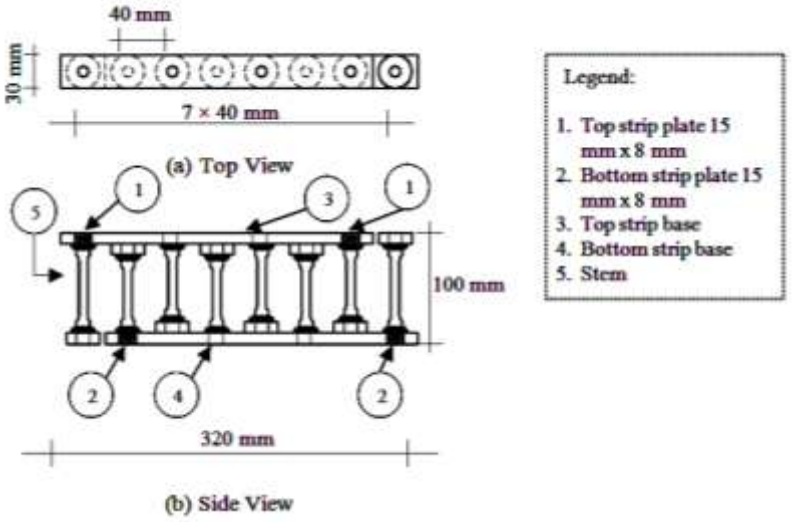

Figure 7 Bottom-up and top-down stud rail of specimen 3 [11].

The first modification of the stud rail was developed for Specimen 2, as shown in Figure 9 [8]. Additional stirrups were placed adjacent to the stems located at both column sides to enhance the torsional capacity of the slab. The use of additional slab stirrups at the column sides is based on the fact that part of the unbalanced moment transferred between column and slab acts as a torsional moment on the side faces of the slab-column joint [14].

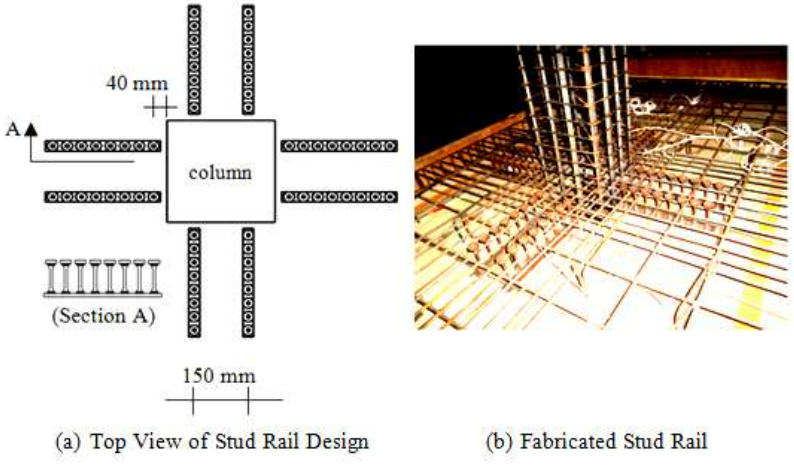

Figure 8 Standard orthogonal stud rail configuration of specimen 1.

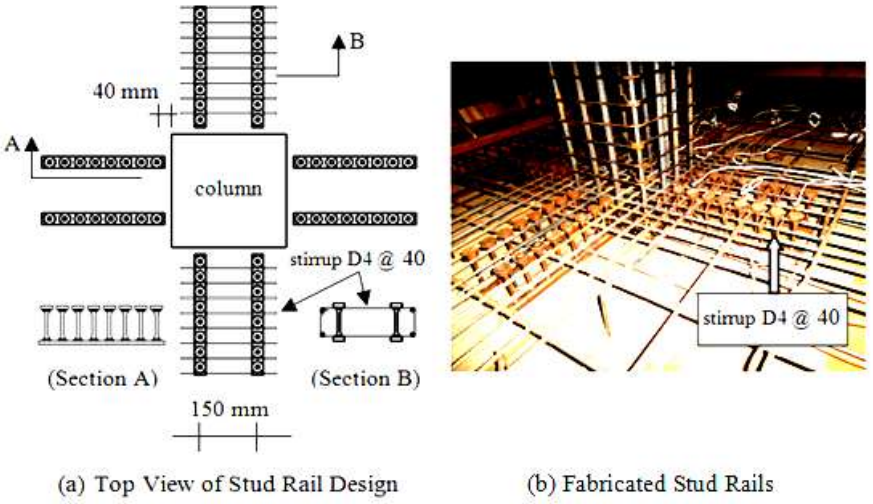

Figure 9 Stud rail and stirrup configuration of specimen 2.

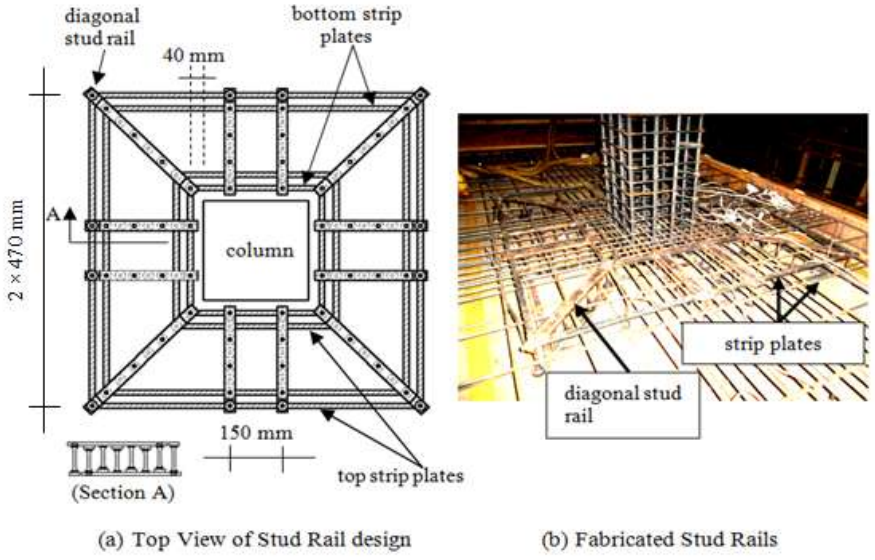

Figure 10 Integrated stud rail of specimen 3.

The second improvement of the stud rail was used for Specimen 3, as shown in Figure 10 [8,11]. Two pairs of diagonal stud rails were arranged along with standard orthogonal stud rails. The stud rails were interconnected using steel strips. This modification was meant to enhance the stiffness and deformation capacity of the slab.

As the third improvement, Specimen 4 was designed similar to Specimen 3, but here the stud rails were un-connected along the perimeter (Figure 11) [8].

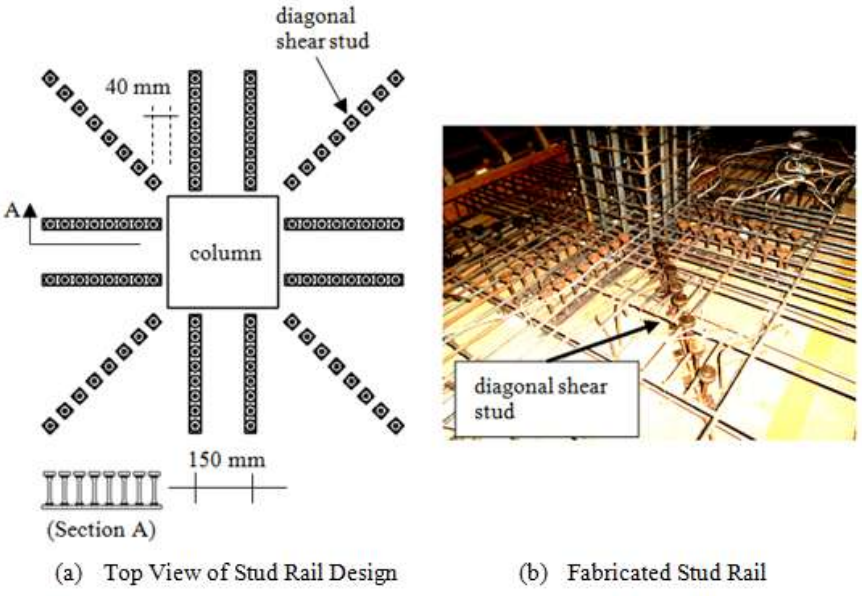

Figure 11 Standard plus diagonal stud rail of specimen 4.

2.3 Instrumentation

The displacement of certain points of the specimens was measured using LVDTs. One LVDT was located at the actuator to record the displacement of the upper tip of the columns. The other LVDTs were located at the roller supports to assure that the supports practically did not move both in transversal and vertical directions. The other instruments used were strain gauges. The strain gauges were located on the slab flexural reinforcement next to the column face and on the stems.

2.4 Loading System

The combined gravity and cyclic lateral loads used in the research are shown in Figure 12 [9]. The total gravity load was 5.70 kPa, which was introduced by

concrete blocks (Figure 12(a) [9]). The gravity load represented 30 percent of the live load, superimposed dead load, and to compensate for the remainder of the self-weight, since the specimens were designed at half scale [6].

Specimen 1 differed in implementing the gravity load. The concrete blocks were hung after all of the roller supports had been fixed. This loading method led to a smaller gravity shear ratio (*GSR*) and the related slab moment (M_g). The concrete blocks of the other specimens were hung before fixing the roller supports, providing a larger initial gravity shear ratio (Table 3 [9,11]) as the gravity load was supported only by the column [6]. However, as the lateral load dominates the structural response, the difference related to the gravity loading should not be significant.

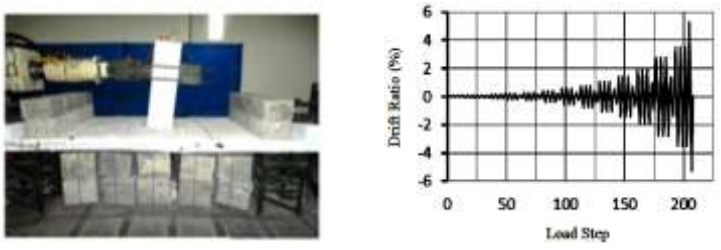

(a) (b)

Figure 12 Combined gravity and cyclic lateral loads (a) and pattern of the cyclic lateral loading (b).

The cyclic lateral load (Figure 12(b) [9]) was generated by an actuator using displacement control (Figure 12(a) [9]). The maximum load of the actuator was 1000 KN, while the maximum displacement was 100 mm. The cyclic load was implemented gradually ranging from elastic to inelastic conditions, represented by drift ratios of 0.06% and 5.25% respectively. The loading was implemented with a very low velocity of 0.03 mm seconds^{-1} to avoid dynamic effects.

Table 3 Initial Gravity Shear Ratio (GSR) of all specimens.

Specimen	Compression Strength, f'_c (MPa)	Gravity Shear Force and Stress at the Critical Section				
		Shear Force, V_u (KN)	Section Area, A_c (10^4mm^2)	Shear Stress, v_{ug} (MPa)	Nominal Stress, v_n (MPa)	*GSR* (%)
(1)	(2)	(3)	(4)	(5)=(3)/(4)	(6)	(7)=(5)/(6)
1	46.21	23.60	15.25	0.15	2.26	6.86
2	46.16	42.86	15.25	0.28	2.26	12.46
3	46.17	43.84	15.25	0.29	2.26	12.74
4	32.72	43.15	15.25	0.28	1.91	14.84

2.5 Test Set Up

The specimens were modeled as typical structural systems (Figure 13 [15]) with the bottom of the specimens pin-supported, while the top ends of the columns were free for lateral and rotational displacement. The test set up is shown in Figure 14 [9].

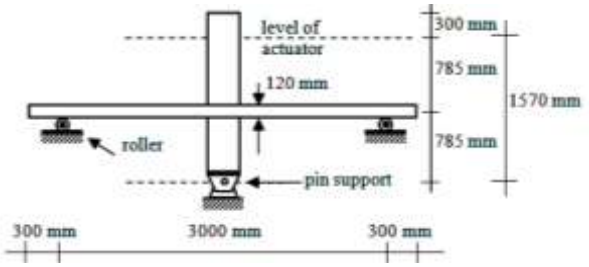

Figure 13 Structural system of the specimens.

Figure 14 Set up of the specimens.

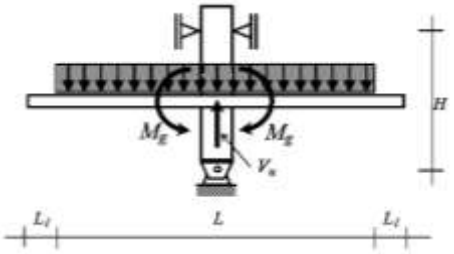

Figure 15 Moment and shear force caused by the gravity load.

Each end of the slabs was supported by a roller to model inflection points at each middle span of the slab of the prototype structures. The rollers were mounted on steel space frames designed to support vertical forces due to the load combination. Even though the steel frames practically do not resist the horizontal load, they were also equipped with diagonal bracings to avoid horizontal displacement. At first, the specimens were designed as columns with cantilever slabs loaded by gravity action. Therefore, in this condition the gravity

load was only supported by the column to maximize the gravity shear ratio [6], as illustrated in Figure 15 [16]. After all of the concrete blocks were hung under the slab, the roller supports were installed.

3 Experimental Results and Discussion

Improvement of specimen behaviors was achieved by the use of additional materials required to develop the stud rail details. Specimen 2 required some stirrups, while Specimen 3 and 4 required 50% extra stems. Strip plates were also required for Specimen 3 to interconnect the stud rails.

3.1 Crack Patterns

The difference in implementing the gravity load caused different initial responses. The larger negative slab moments on Specimens 2, 3, and 4 led to initial cracks on the slab top surface (Figure 16 [8,9,11]).

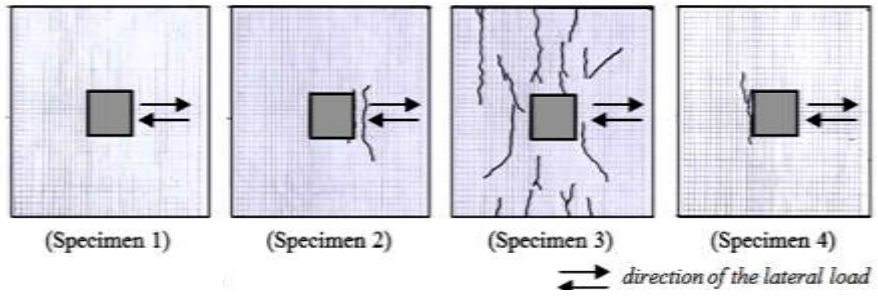

Figure 16 Initial crack patterns (drift ratio of 0%) of all specimens.

On the other hand, no initial cracking occurred in Specimen 1 under the gravity load. Figure 16 also shows the different crack patterns in Specimens 2, 3, and 4, although the gravity loads were similar, indicating the effect of the different stud rail details on the crack patterns.

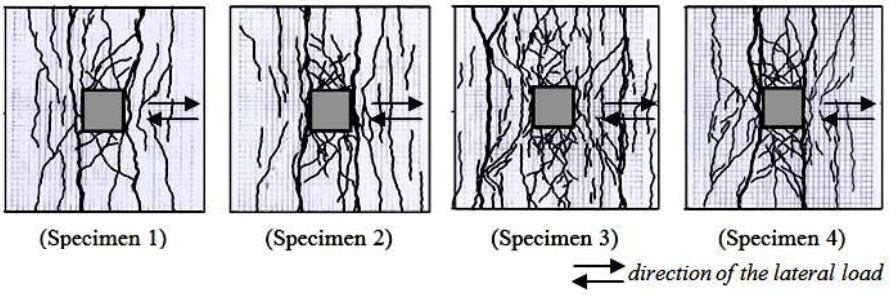

Figure 17 Final crack patterns (drift ratio of 5.25%) of all specimens.

Tests were then conducted using combined gravity and cyclic lateral loads. The final crack patterns (at a drift ratio of 5.25%) are shown in Figure 17 [8,9,11]. The main cracks on the slabs of Specimens 1, 2, and 4 occurred near the column faces, while the main cracks on the slab of Specimen 3 occurred near the outer ends of the shear reinforcement.

3.2 Hysteretic Curves

The hysteretic behavior of the specimens as a relation between the lateral load and upper end column displacement is shown in Figure 18 [8,9,11]. All specimens were subjected to three cycles of lateral load for each drift ratio (Figure 12 (b)), except for drift ratio of 5.25%. Each specimen showed very good hysteretic behavior. The hysteretic loops within each drift ratio were close to each other, indicating that no significant stiffness or strength degradation occurred during the three-cycle loading at each drift ratio.

The overall situation indicated that the average peak lateral force of Specimen 3 reached at drift ratio 5.25% was superior compared to those of the other specimens. The hysteretic curve of Specimen 2 was off from the origin because of the un-symmetric initial crack (Figure 16) and the direction of the initial lateral load that maximized the tension at the top surface of the slab next to the column.

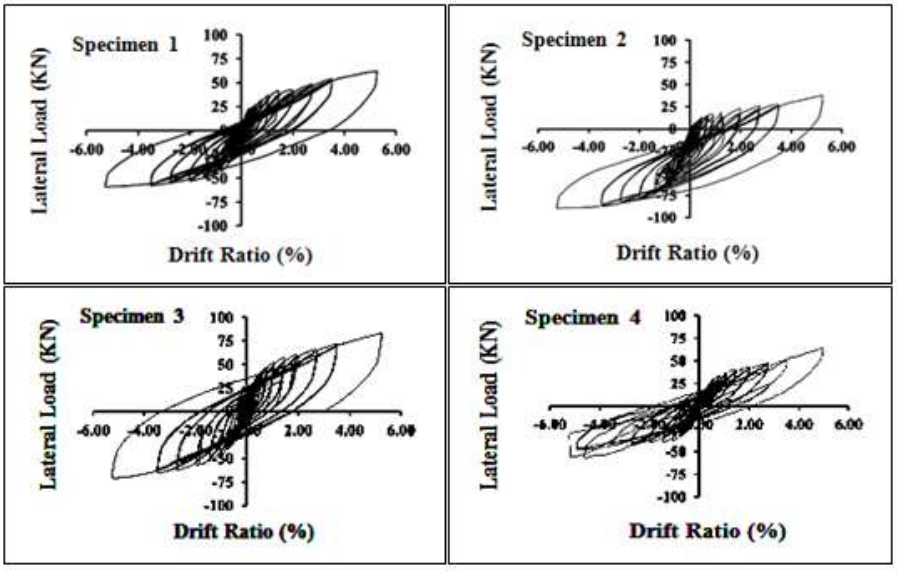

Figure 18 Hysteretic curves of all specimens.

3.3 Strain on Slab Flexural and Shear Reinforcement

The strains of slab flexural and shear reinforcements (Figures 19 and 20) were obtained from the strain gauge readings. The figures do not represent all strain data because of some damage to the strain gauges. Figure 19 shows that the flexural slab reinforcements of the three specimens responded consistently to the cyclic lateral loads. The reinforcement bars were yielding at the peak lateral loading for each loading cycle consistently. No significant bond slip was observed during the loading. The shift of the hysteretic strain to the right indicates the yielding of the reinforcement bars at the plastic hinge areas. No significant slippage of the flexural bars was confirmed, since no cracks developed at the joint. Also, no pinching was observed in the hysteretic curves, which supports the observation that there was no significant bond slip during the test. Figure 20 shows that the stem of Specimen 3 experienced the largest strain and the most consistent shape of hysteretic curve during the test, indicating that it worked more effectively compared to those of the other specimens.

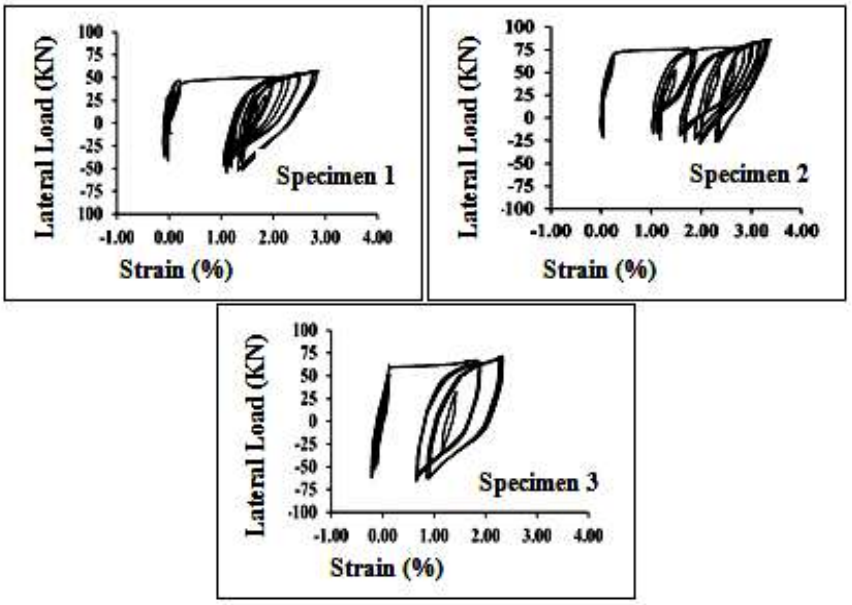

Figure 19 Strain (SG-1) reading on slab top reinforcements.

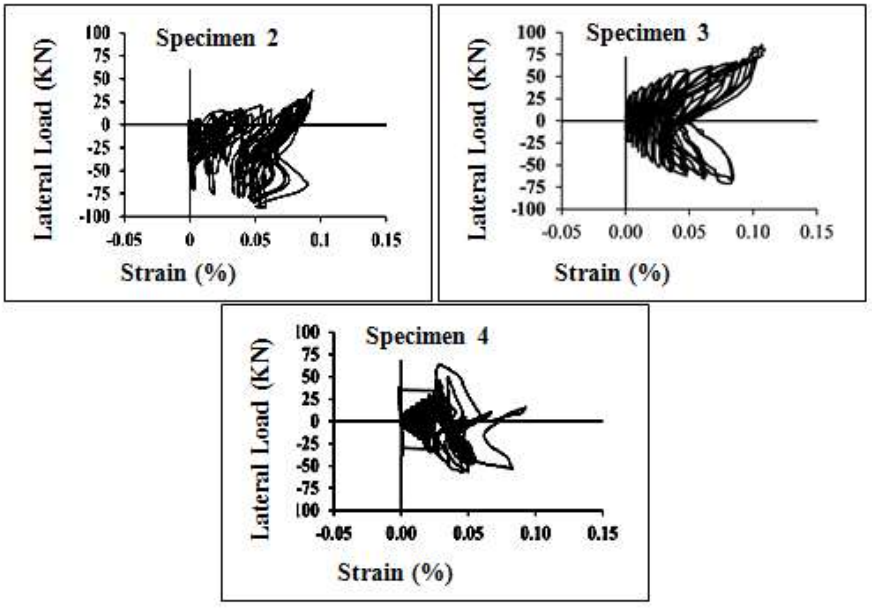

Figure 20 Strain (SG-2) reading on stems.

3.4 Adequacy of Initial Stiffness

A structure is categorized as having an adequate initial stiffness when its lateral resistance obtained from experimental work under the initial drift limit (*IDL*) is larger than its nominal strength [3], which is defined as the negative nominal bending moment of the slab next to the column face. The allowable story drift for buildings of Risk Categories I/II, III, and IV is 0.020, 0.015, and 0.010 times its column height, respectively [4,17,18]. The *IDL* of all specimens for Risk Categories I/II and III (Table 4) was calculated using a deflection amplification factor C_d of 5.5 for dual systems with special moment frames [4,17] and a strength reduction factor ϕ of 0.9 for bending moment [2]. The *IDL* was used to determine the lateral force (F_{exp}) from the hysteretic curve obtained from the experimental work (Figure 21) under combined gravity and lateral loads. The multiplication of F_{exp} and the column height measured from the center of the joint results in the unbalanced moment (M_{exp}) transferred to the slab. The total bending moment (M_{total}), representing lateral resistance under the *IDL*, was obtained as a combination of M_{exp} and the gravity bending moment (M_g). Considering that F_{exp} was obtained under a very small drift ratio (column 3 of Table 4), where the major part of the structure behaved elastically, M_g was calculated based on the initial condition of the structure.

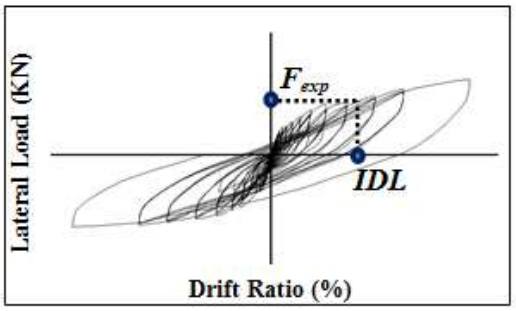

Figure 21 Theoretical position of Initial Drift Limit (*IDL*) and related lateral load (F_{exp}) on hysteretic curve.

The designed nominal bending moments (M_n) were calculated involving the slab within the column strip. Therefore, the contribution of the strip plates of Specimen 3, which were located outside the column strip, was neglected. Besides, the length of the strip plates was not sufficient to transfer the bond stress. The ratios of M_{total} to M_n of all specimens are presented in Table 4. The table shows that Specimens 2, 3, and 4 behaved better than Specimen 1. Specimen 2, 3, and 4 fulfilled the requirement of initial stiffness designed for Risk Category I/II, indicated by ratios larger than 100%. Specimen 3 was the only specimen that also fulfilled the initial stiffness requirement designed for Risk Category III.

Table 4 Ratio of slab bending moment to nominal moment at initial drift limit.

Risk Category	Specimen	Initial Drift Limit (%)	Experimental Results				M_n (10 KN.m)	Ratio of M_{total}/M_n (%)
			F_{exp} (KN)	M_{exp} (10 KN.m)	M_g (10 KN.m)	M_{total} (10 KN.m)		
(1)	(2)	(3)	(4)	(5)=(4)*h/2	(6)	(7)=(5)+(6)	(8)	(9)=(7)/(8)
I/II	1	0.40	23.88	1.87	0.39	2.27	2.32	97.94
	2	0.40	22.96	1.80	0.72	2.52	2.32	108.90
	3	0.40	29.30	2.30	0.74	3.04	2.32	131.19
	4	0.40	23.83	1.87	0.72	2.59	2.20	117.61
III	1	0.30	19.45	1.53	0.39	1.92	2.32	82.93
	2	0.30	20.03	1.57	0.72	2.29	2.32	98.97
	3	0.30	23.56	1.85	0.74	2.59	2.32	111.74
	4	0.30	18.81	1.48	0.72	2.20	2.20	99.73

3.5 Stiffness Degradation

The results of the evaluation of stiffness degradation are shown in Table 5. The degraded stiffness ($K_{3.5}$) should not be less than 5% of the initial stiffness (K_0) [10] because a very small degraded stiffness leads the structure to be vulnerable to major earthquakes.

Table 5 Evaluation of the stiffness degradation ratio.

Specimen	Positive Direction			Negative Direction			Average
	K_o	$K_{AA'}$	$K_{AA'}/K_o$ (%)	K_o'	$K_{BB'}$	$K_{BB'}/K_o'$ (%)	$K_{3.5}/K_o$ (%)
	(10^2 N/mm)			(10^2 N/mm)			
(1)	(2)	(3)	(4)=(3)/(2)	(5)	(6)	(7)=(6)/(5)	(8)=((4)+(7))/2
1	75.50	7.11	9.42	126.00	7.35	5.83	7.63
2	86.00	7.43	8.64	86.00	7.28	8.47	8.55
3	124.00	8.49	6.84	95.80	8.63	9.01	7.93
4	60.60	6.51	10.75	78.50	8.22	10.47	10.61

The initial stiffness (K_o) is defined as the stiffness of the first cycle under a drift ratio of 0.06%. The degraded stiffness is defined as the slope of the line connecting point A to point A' for positive (loading) direction and the line connecting point B to point B' for negative (reloading) direction [10] (Figure 22). Point C and D indicate drift ratios of -0.35% and +0.35% respectively. Table 5 shows that the stiffness degradation represented by the ratios $K_{AA'}/K_o$ and $K_{BB'}/K_o'$ for all specimens was not less than the standard limitation [10]. The development of the stud rail increased the average stiffness degradation ratio ($K_0/K_{3.5}$) effectively for all three specimens, especially Specimen 4.

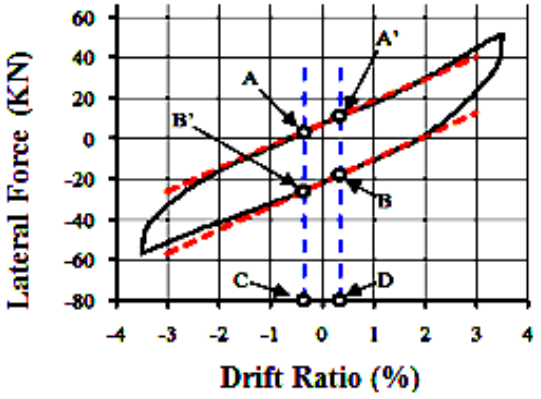

Figure 22 Stiffness around zero drift ratios defined using third cycle of drift ratio 3.50%.

3.6 Energy Dissipation

To prevent inadequacy of hysteretic damping, the relative energy dissipation ratio, which is defined as the ratio of the energy of the last cycle under a drift ratio of 3.50% to the energy of the elastoplastic model (Figure 23), should not be less than 12.5 percent [10]. It was found that the initial stiffness K_o (the slope of line 0-1) and K'_o (the slope of line 0-2), for positive and negative lateral forces respectively, were different.

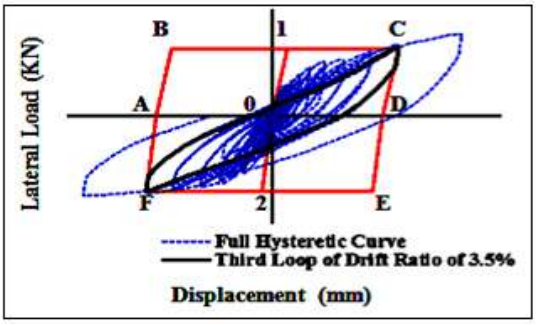

Figure 23 Energy dissipation ratio of third cycle under 3.50% drift ratio.

The relative energy dissipation ratio (Table 6) is calculated as the hysteretic energy (represented by the area of the third loop under a drift ratio of 3.50%), divided by the energy under elastoplastic conditions (represented by the sum of the areas of parallelograms ABCD and DEFA), as shown in Figure 23. The slopes of lines AB and DC were equal to the initial stiffness K_o for positive loading, while the slopes of lines DE and AF were equal to the initial stiffness K'_o for negative loading. The relative energy dissipation ratios of all specimens exceeded the minimum ratio of 12.5%. The larger relative energy dissipation ratios of Specimens 2 and 3 proved that the new designs of the shear reinforcement details significantly improved the energy dissipation.

Table 6 Evaluation of energy dissipation.

Specimen	Initial Stiffness		Lateral Force under 3.50% Drift Ratio		Energy Dissipation of the 3rd Cycle Loop	Total area of [ABCD] + [DEFA]	Ratio of Relative Energy Dissipation (%)
	K_o	K'_o	Positive	Negative			
	(10^3N/mm)		(KN)		(KN.m)		
(1)	(2)	(3)	(4)	(5)	(6)	(7)	(8)=(6)/(7)
1	7.55	12.62	51.35	-56.12	2.76	10.63	25.94
2	8.60	8.60	25.14	-82.13	3.50	10.46	33.46
3	12.39	9.58	70.65	-61.53	4.37	12.94	33.82
4	6.06	7.85	48.98	-42.31	2.17	8.79	24.73

4 Conclusions

The experimental results provide some information related to the improvement of the behavior of the slab-column connections with newly designed stud rail details. It was found that there was no significant slippage of the flexural reinforcement in the connections throughout the cyclic test. Each specimen produced very good hysteretic behavior.

The newly designed stud rail details significantly improved the behavior of the slab-column connections in terms of initial stiffness, stiffness degradation, and energy dissipation. The highest ratios of the experimental bending moment under *IDL* (M_{total}) to the nominal bending moment (M_n), used to evaluate the adequacy of initial stiffness, were 131.19% for Risk Category I/II and 111.74% for Risk Category III as demonstrated by Specimen 3, compared to a ratio of 97.94% for Risk Category I/II and a ratio of 82.93% for Risk Category III as demonstrated by the Control Specimen. The highest ratio of stiffness degradation was 10.61% as demonstrated by Specimen 4, compared to a ratio of 7.63% as demonstrated by the Control Specimen. The highest ratio of relative energy dissipation was 33.82% as demonstrated by Specimen 3, compared to a ratio of 25.94% as demonstrated by the Control Specimen. Overall evaluation shows that Specimen 3 provided the best behavior under combined gravity and cyclic lateral loads.

Based on the evidence that the newly designed stud rail details significantly improve the behavior of slab-column connections, it is possible to design and construct tall buildings using dual systems consisting of slab-column frames as Special Moment Frames and structural walls. Furthermore, flat slab structures as Special Moment Frames can be constructed as dual systems with no limitations related to seismic zones.

Acknowledgements

The authors would like to express their deep appreciation and gratitude to the officials of the ITB I-MHERE PROGRAM 2011 that has funded this research. The appreciation and gratitude are also extended to the head and technicians of the Structural Mechanics Laboratory of the Engineering Center for Industry of the Institut Teknologi Bandung, who contributed invaluable assistance in making this research possible.

References

[1] Hueste, M.B.D., Browning, J.A., Lepage, A. & Wallace, J.W., *Seismic Design Criteria for Slab-Column Connections*, ACI Structural Journal, **104**(4), pp. 448-458, 2007.

[2] ACI Committee 318, *Building Code Requirements for Structural Concrete (ACI 318M-11) and Commentary*, American Concrete Institute, Farmington Hills, Michigan, USA, 2011.
[3] Badan Standarisasi Nasional, *The Design Method of Concrete Structure for Buildings* (*SNI 03-2847-2002*), Badan Standarisasi Nasional, Jakarta, 2002.
[4] American Society of Civil Engineers, *Minimum Design Loads for Buildings and Other Structures (ASCE/SEI 7-10)*, American Society of Civil Engineers, Reston, Virginia, USA, 2010.
[5] Megally, S. & Ghali, A., *Punching Shear Design of Earthquake-Resistant Slab-Column Connections*, ACI Structural Journal, **97**(5), pp. 720-730, 2000.
[6] Robertson, I.N., Kawai, T., Lee, J. & Enomoto, B., *Cyclic Testing of Slab-Column Connections with Shear Reinforcement,* ACI Structural Journal, **99**(5), pp. 605-613, 2002.
[7] Broms, C.E., *Ductility of Flat Plates: Comparison of Shear Reinforcement System*, ACI Structural Journal, **104**(6), pp. 703-711, 2007.
[8] Budiono, B., Imran, I., Sofwan, A. & Gunadi, R., *The Hysteretic Behavior of Slab-Column Connection Sub-Assemblages with Shear Reinforcement under Cyclic Lateral Load*, Research Report, Institut Teknologi Bandung, Bandung, 2012.
[9] Gunadi, R., Budiono, B., Imran, I., & Sofwan, A., *Experimental Study on the Behavior of Slab-Column Connections under Combined Gravity and Cyclic Lateral Loads*, Jurnal Teknik Sipil-ITB, **19**(3), pp. 195-205, 2012.
[10] ACI Committee 374, *Acceptance Criteria for Moment Frames Based on Structural testing and Commentary (ACI 374.1-05)*, American Concrete Institute, Farmington Hills, Michigan, USA, 2005.
[11] Gunadi, R., Budiono, B., Imran, I. & Sofwan, A., *Experimental Study on the Behavior of Slab-Column Connections using New Shear Reinforcement Detail*, Proceeding, The 6th Civil Engineering Conference in Asia Region, Jakarta, Indonesia, August 20-22, pp. TS2.1-8, 2013.
[12] ACI-ASCE Committee 352, *Recommendations for Design of Slab-Column Connections in Monolithic Reinforced Concrete Structures (ACI 352.1R-89)*, American Concrete Institute, Farmington Hills, Michigan, USA, 2004.
[13] Joint ACI-ASCE Committee 421, *Shear Reinforcement for Slabs (ACI 421.1R-99)*, American Concrete Institute, Farmington Hills, Michigan, USA, 1999.
[14] Alexander, S.D.B. & Simmonds, S.H., *Moment Transfer at Interior Slab-Column Connections*, ACI Structural Journal, **100**(2), pp. 197-202, 2003.
[15] Gunadi, R., Budiono, B., Imran, I. & Sofwan, A., *Numerical Analysis: The Behavior of Slab-Column Connections with New Shear*

Reinforcement Detail Subjected to Combined Gravity and Cyclic Lateral Loads, The 2nd Indonesian Structural Engineering and Materials Symposium, Bandung, Indonesia, November 7-8, pp. T11.1-12, 2013.

[16] Gunadi, R., Budiono, B., Imran, I. & Sofwan, A., *Numerical Analysis: Enhancing the Behavior of Slab-Column Connections by Improving the Shear Reinforcement Detail*, BIGSTAR (Building International Gateway through Science, Technology, and Arts) International Conference, Bandung, Indonesia October 28-29, pp. 216-225, 2013.

[17] American Society of Civil Engineers, *Minimum Design Loads for Buildings and Other Structures (ASCE 7*-05), American Society of Civil Engineers, Reston, Virginia, USA, 2006.

[18] International Code Council, *International Building Code (IBC 2000)*, International Code Council, Inc., Country Club Hills, Illinois, USA, 2000.